https://doi.org/10.5194/egusphere-2026-385
Preprint. Discussion started: 29 January 2026
© Author(s) 2026. CC BY 4.0 License.

Mean Energy variation of Diffuse Aurora Observed with the ASIS Spectrograph

Gaël Cessateur[1], Keisuke Hosokawa[2,3], Hervé Lamy[1], Sota Nanjo[4], Mathieu Barthelemy[5], Magnar G. Johnsen[6], and Romain Maggiolo[1]

[1]Royal Belgian Institute for Space Aeronomy, Avenue Circulaire 3, 1180 Brussels, Belgium
[2]Department of Communication Engineering and Informatics, University of Electro-Communications, Tokyo, Japan
[3]Center for Space Science and Radio Engineering, University of Electro-Communications, Tokyo, Japan
[4]Swedish Institute of Space Physics, IRF Kiruna, 981 92 Kiruna, Sweden
[5]Univ. Grenoble Alpes, CNRS, IPAG, 38000 Grenoble, France
[6]Tromsø Geophysical Observatory, Faculty of Science and Technology, UiT the Arctic University of Norway, N-9037 Tromsø, Norway

Correspondence: Gaël Cessateur: gael.cessateur@aeronomie.be

Abstract. We analyze more than 20,000 spectra of diffuse aurora recorded by the ASIS spectrograph over two winters, focusing on events classified as diffuse by an AI-based system, which includes pulsating auroras as a major subset. Electron characteristic energies were derived from calibrated red/blue emission ratios using a lookup-table approach based on forward modeling. To assess the systematic evolution of these energies with magnetic local time (MLT), we applied a Bayesian regression framework to the median of the mean-energy estimates, providing a robust characterization despite the large intrinsic variability of diffuse precipitation. The results reveal a clear hardening of the precipitation toward the dawn sector. Using the AE index as a proxy for geomagnetic activity, we further show that the MLT-dependent trend is influenced not only by the instantaneous AE level but also by the recent magnetospheric history, as revealed by time-lagged classifications. These findings indicate that diffuse auroral precipitation retains an imprint of preceding magnetospheric dynamics and are consistent with chorus-wave scattering modulated by evolving plasma-sheet conditions.

1 Introduction

Diffuse auroras frequently display quasi-periodic intensity modulations known as ON–OFF switching, with periods ranging from a few to several tens of seconds commonly referred to as pulsating auroras (PsAs) (Yamamoto, 1988; Royrvik and Davis, 1977). PsAs are typically observed in the post-midnight to morning sectors during the recovery phase of substorms and are typically associated with moderately disturbed geomagnetic conditions (Hosokawa and Ogawa, 2015; Partamies et al., 2017; Nishimura et al., 2010a). Early ground-based optical observations, combined with very-low-frequency (VLF) wave measurements, suggested that PsAs are produced by pitch-angle scattering of energetic electrons by whistler-mode chorus waves (e.g. Tsuruda et al., 1981; Ozaki et al., 2012). This interpretation has been firmly reinforced through numerous conjugate observations combining ground-based optical instruments and in-situ satellite measurements, demonstrating that PsAs originate

https://doi.org/10.5194/egusphere-2026-385
Preprint. Discussion started: 29 January 2026
© Author(s) 2026. CC BY 4.0 License.

from wave–particle interactions between energetic electrons and chorus waves in the magnetosphere (e.g. Nishimura et al., 2010b; Kasahara et al., 2018; Ozaki et al., 2019; Hosokawa et al., 2020).

Whistler-mode chorus waves are electromagnetic waves typically generated near the geomagnetic equator in the frequency range of 0.1 to 0.8 times the electron cyclotron frequency ($f_{ce} = \frac{qB}{2\pi m_e}$), with a gap at 0.5 f_{ce} separating the lower and upper chorus bands. These waves propagate along magnetic field lines and can interact resonantly with energetic electrons through the cyclotron resonance condition:

$$\omega - k_{\parallel} v_{\parallel} = \frac{n f_{ce}}{\gamma} \tag{1}$$

where ω is the wave frequency, $k_{\parallel}$ is the parallel wave number, $v_{\parallel}$ is the electron velocity along the magnetic field, n is the resonance harmonic number (± 1 for fundamental resonance), and γ is the Lorentz factor. Using a kinetic modeling approach based on bounce-averaged diffusion, Miyoshi et al. (2015) demonstrated that lower-band chorus waves preferentially resonate with higher-energy electrons, producing intermittent high-energy precipitation characteristic of PsAs, whereas upper-band chorus waves primarily generate more stable and softer diffuse precipitation. In addition to chorus waves, other plasma waves can also contribute to diffuse auroral precipitation. In particular, electrostatic electron cyclotron harmonic (ECH) waves have been shown to scatter electrons with energies of a few keV into the loss cone. In-situ observations by the Arase satellite revealed a statistically significant correlation between ECH wave activity near the magnetic equator and enhanced loss-cone electron fluxes at energies around several keV, sufficient to generate observable auroral emissions (Fukizawa et al., 2020). Although ECH waves are not considered the primary driver of PsAs, these results indicate that multiple wave modes may influence the energy distribution of electrons precipitating in diffuse auroral regions.

Extensive ground-based observations have provided important constraints on the spatial and temporal characteristics of PsAs and diffuse auroras. Incoherent-scatter radar measurements with the European Incoherent SCATter (EISCAT) radar have provided altitude-resolved electron density profiles during PsAs events, indicating multi-keV electron precipitation peaking near 100–110 km and significant ionospheric conductivity changes (Hosokawa and Ogawa, 2015). High-cadence optical observations using narrow-field photometers and high-speed cameras have resolved fine-scale temporal modulations and localized precipitation structures on spatial scales of a few to several tens of kilometers (Nishimura et al., 2010b; Nozawa et al., 2018). Wide-field all-sky imager (ASI) networks have documented the large-scale morphology, spatial structuring, and horizontal drift of diffuse and pulsating auroral forms over broad regions of the auroral oval, enabling statistical studies of their occurrence and evolution across MLT (Donovan et al., 2006; Nanjo et al., 2021; Hosokawa et al., 2023). These ASI observations primarily constrain auroral morphology and dynamics, without providing direct measurements of electron precipitation energy.

Satellite observations have also played a crucial role in establishing the magnetospheric origin of pulsating and diffuse auroral precipitation. Kasahara et al. (2018) provided direct in-situ evidence linking magnetospheric chorus-wave activity with electron precipitation causing PsAs, demonstrating a clear one-to-one correlation between lower-band chorus wave enhancements and corresponding electron flux modulations in the atmosphere. Specifically, Kasahara et al. (2018) observed a close temporal correlation between the spacecraft-measured magnetic wave power spectral density (PSD) of lower-band chorus

https://doi.org/10.5194/egusphere-2026-385
Preprint. Discussion started: 29 January 2026
© Author(s) 2026. CC BY 4.0 License.

waves and the flux of precipitating electrons in the loss cone. The observed correlation confirmed that lower-band chorus waves play a pivotal role in modulating both the flux and energy distribution of electrons precipitating into Earth's atmosphere, leading to the characteristic pulsating aurora emissions. Using high-speed ground-based optical cameras in conjunction with in-situ measurements from the Arase satellite, Hosokawa et al. (2020, 2023) demonstrated a clear temporal correspondence between fine-scale auroral luminosity modulations and magnetospheric wave-related electric-field fluctuations. Their results provide strong evidence for a causal link between magnetospheric wave–particle interactions and the modulation of auroral precipitation. Nanjo et al. (2023) also reported conjugate observations combining Arase measurements and all-sky imagers, revealing internal modulations within individual pulsating auroral patches and their close association with magnetospheric wave activity.

The characteristic energy of electron precipitation associated with PsAs typically spans the range from several tens to several hundreds of keV, leading to enhanced emissions in the green oxygen line at 557.7 nm and the blue N_2^+ band at 427.8 nm (Kawamura et al., 2020). Several observational studies have suggested that both the peak emission altitude and the characteristic energy of precipitating electrons vary systematically with MLT, with a general trend toward harder precipitation and lower emission altitudes in the post-midnight and dawn sectors (Newell et al., 2009; Kawamura et al., 2020; Nanjo et al., 2021). From a magnetospheric perspective, this trend can be interpreted in terms of changes in chorus wave properties with MLT. In particular, Ito et al. (2024) showed that chorus waves observed in the dawn sector tend to occur in regions with lower local electron cyclotron frequencies and exhibit larger $k_{\parallel}$ than those observed closer to midnight. These properties shift the resonance condition toward higher-energy electrons, helping to explain the increased mean precipitation energy. This effect arises not from the magnetic field strength B alone, but from the combined influence of wave parameters and plasma environment. In particular, a lower ratio of ω/f_{ce} and a higher $k_{\parallel}$ value tend to increase the resonant parallel velocity $v_{\parallel}$ of the electron, i.e. selecting higher-energy electrons for interaction.

Despite the strong observational and theoretical evidence linking PsAs and diffuse auroral precipitation to wave–particle interactions, the systematic evolution of electron precipitation energy across MLT remains incompletely characterized. Most previous studies have relied on imaging or radar techniques that provide limited spectral information or indirect energy proxies. Continuous spectroscopic observations with sufficient temporal resolution remain comparatively scarce. In this study, we use high-cadence ground-based auroral spectroscopy to infer the mean energy of precipitating electrons using emission-line intensity ratios (Adachi et al., 2017), enabling a statistical investigation of energy variations in diffuse auroras as a function of magnetic local time.

2 Data & Methods

2.1 Spectral Data

Auroral spectra were collected using the Auroral Spectrograph In Skibotn (ASIS), a high-cadence spectrograph located within the auroral oval at the field station of UiT – The Arctic University of Norway in Skibotn (69.34°N, 20.36°E). Operational since October 2023, ASIS has a relatively wide field of view (FoV) of approximately 4°. Spectral intensity is integrated over the

https://doi.org/10.5194/egusphere-2026-385
Preprint. Discussion started: 29 January 2026
© Author(s) 2026. CC BY 4.0 License.

entire entrance slit, enhancing the signal, but limits spatial resolution. The instrument is fixed in an orientation aligned with the local geomagnetic field lines (elevation 77.2°, azimuth 182.8°) to optimize the detection of auroral emissions along the direction of electron precipitation. A 300 grooves/mm grating is used to record spectra throughout the 405–687 nm range, with a temporal resolution of 30 seconds, allowing detailed monitoring of auroral variability, taken only during the astronomical night (solar zenith angle > 108°). All spectra were calibrated in spectral radiance units (R/nm). Emission intensities were then derived from the calibrated spectra: the blue N_2^+ emission was obtained by integrating the spectrum over the 425–429 nm interval, after subtraction of a local continuum estimated as the mean signal in the adjacent 430–435 nm band. The red oxygen emission at 630 nm was calculated by integrating the continuum-subtracted spectrum over the 628–632 nm interval, where the local baseline was approximated by the mean of the intensities at the two edges of the integration window.

To ensure robust auroral spectra, only measurements with a blue-band intensity greater than 100 R were retained. This empirically defined threshold primarily suppresses background-dominated conditions and also removes very low-intensity auroral events, typically associated with weak and low-energy electron precipitation. The latter are not central to the present study, which focuses on relative variations of electron energy during well-developed auroral activity.

To identify spectra specifically corresponding to diffuse auroras, we employed the machine-learning-based classification method developed by Nanjo et al. (2022). This system uses color all-sky images captured every 30 seconds with an 8-second exposure by a Sony Alpha 6400 (ILCE-6400) camera equipped with a Meike MK-6.5mm F2.0 fisheye lens. The classifier distinguishes between several auroral categories: “Arc,” “Discrete,” “Diffuse,” “Noisy aurora,” and “No aurora.” Figure 1 shows an example keogram for a typical night, from the 14th to the 15th December 2023, illustrating the temporal distribution of auroral emissions. Diffuse auroras are especially prominent in the dusk and dawn sectors.

According to Nanjo et al. (2022), diffuse auroras are characterized by spatially extended, weakly structured emissions, distinct from discrete and highly structured auroral forms. Within this general class, several subtypes have been identified in previous studies (e.g. Nishimura et al. (2020); Grono and Donovan (2018)): (i) Pulsating auroras (PsAs), showing quasi-periodic luminosity modulations on timescales of a few to tens of seconds, which are the focus of this study; (ii) Patchy diffuse auroras, consisting of stable or slowly varying emission patches often drifting with magnetospheric convection; (iii) Amorphous diffuse auroras, characterized by unstructured, irregular luminosity without obvious periodicity; and (iv) Diffuse veiling auroras, broad and faint luminosity layers forming a background to other types. In the present study, we consider all these types collectively as “diffuse aurora,” with pulsating auroras forming a major but not exclusive subgroup.

A total of more than 20,000 spectra were analyzed from October 2023 to March 2024, then October 2024 to March 2025. Only time intervals classified as ’Diffuse’ with a confidence level greater than 75% and lasting at least 5 minutes were selected for further analysis, ensuring that the data set reflects stable and well-identified diffuse/pulsating auroral activity. We do have more than 1000 events per month, except for February 2024 and March 2025 which were predominantly cloudy.

Figure 2 represents the number of individual spectra classified as diffuse auroras, distributed per hourly binned MLT, approximated here as UT + 2.5 h for the Skibotn observatory location. Diffuse auroras occur throughout the entire night, with a slightly higher occurrence in the morning sector than in the evening sector. Nevertheless, the number of events remains significant across all MLT bins, exceeding 500 events per bin between 20 and 07 MLT.

https://doi.org/10.5194/egusphere-2026-385
Preprint. Discussion started: 29 January 2026
© Author(s) 2026. CC BY 4.0 License.

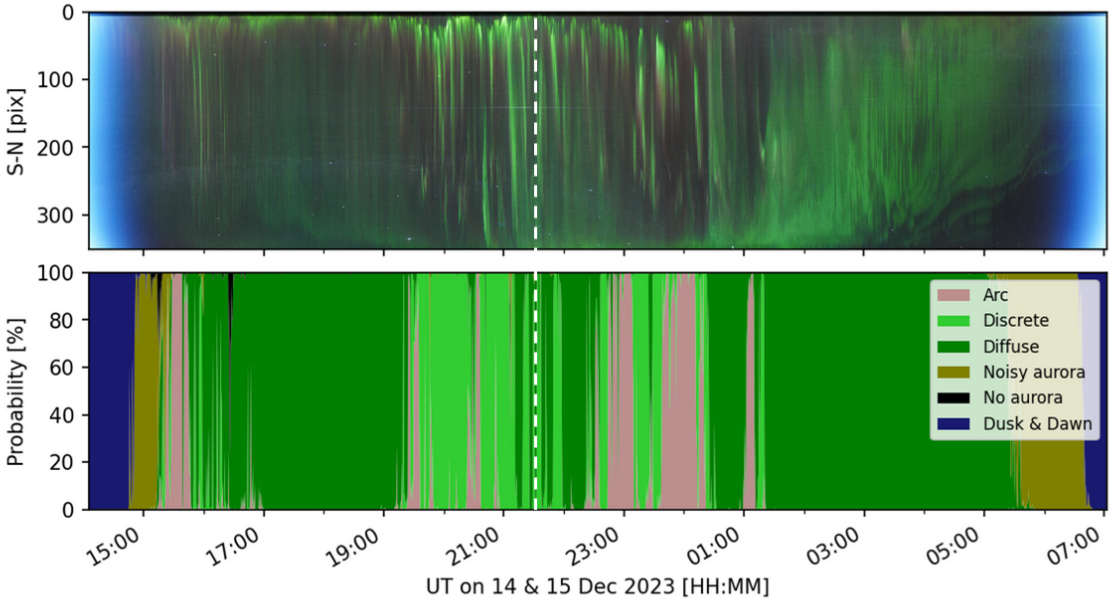

Figure 1. Example keogram for 14–15 December 2023 showing the temporal evolution of auroral emissions (top panel) and the corresponding AI-based auroral-classification probabilities (bottom panel). Only intervals labeled as "Diffuse" with classification confidence greater than 75% and lasting at least 5 minutes were retained for analysis. Vertical white dashed-line represents the magnetic midnight.

2.2 Energy Inference via Line Ratio

The mean energy of precipitating electrons is estimated using the look-up tables provided by Adachi et al. (2017), which assume a Maxwellian electron energy distribution and are based on kinetic electron transport modeling with the "GLobal airglOW model" (GLOW) (Solomon, 2017). The intensity ratio between the red (630.0 nm) and blue (427.8 nm) auroral lines, as shown in Figure 1 from Adachi et al. (2017), serves as a proxy for the mean electron energy, and higher ratios indicate softer precipitation within the framework of the lookup-table models. We also tried another kinetic electron transport model, Transsolo (Barthelemy et al., 2025) with a monoenergetic precipitating electron flux, using up to 32 streams, while GLOW uses only 2 streams. These models are stationary and are therefore only valid where the quasi-steady-state hypothesis holds, such as in quiet steady arcs and diffuse auroras (Adachi et al., 2017).

Figure 3 shows two representative ASIS spectra acquired during the same night as Figure 1. The first spectrum was recorded before midnight, at 18:10:11 UT on 14 November, while the second was obtained after midnight, at 02:54:16 UT on 15 November. These two spectra illustrate the marked spectral differences observed between the early evening and post-midnight periods. Using the red-to-blue intensity ratio and the lookup-table method, the characteristic electron energy is estimated to be

https://doi.org/10.5194/egusphere-2026-385
Preprint. Discussion started: 29 January 2026
© Author(s) 2026. CC BY 4.0 License.

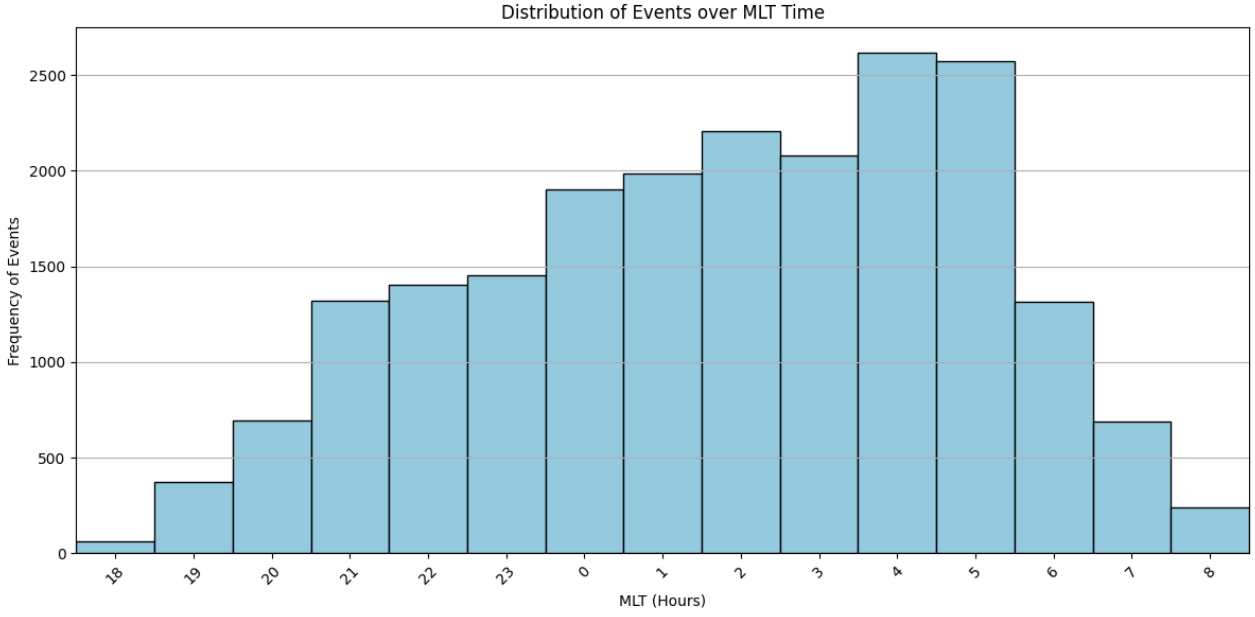

Figure 2. Number of diffuse-aurora spectra per 1-hour MLT bin used in the statistical analysis

approximately 2.5 keV before midnight, with red and blue emissions of about 1700 R and 720 R, respectively. After midnight, the inferred characteristic energy increases to roughly 6.2 keV, corresponding to red and blue emissions of approximately 2430 R and 3800 R. In the higher-energy case, the N_2^+ First Negative (1N) system becomes more pronounced: the (0–1) band at 427.8 nm and the (0–2) band near 470.9 nm both intensify, together with the N_2 Meinel band emissions between 650 and 680 nm. These features are characteristic signatures of increased electron energies in auroral precipitation.

Figure 4 shows the estimated characteristic average energy for the same night, for both GLOW (in blue) and TRANSSOLO (in green) approaches. While the latter approach underestimates the average energy, both approaches share the same variability, highlightening the differences between the dusk and dawn sectors in this specific night case. While the absolute value might differ, the variability trend over the night should be consistent with both approaches. We then limit ourselves to the mean energy estimation using the look-up tables provided by Adachi et al. (2017). Figure 4, panel d), shows the external magnetic field variations at the nearby Tromsø Magnetic Observatory. The variations show that our observations are performed below the eastward electrojet prior to about 20 UT, where the change of sign indicates transition through the Harang discontinuity. Several small negative bays are seen indicating substorm or pseudo breakup activity, before the stations sees clear westward electrojet conditions after 0 UT. The amplitudes of the magnetic activity (+/- 100-150 nT) taken into account, this may be considered an "ordinary" or quiet time event within the statistical auroral oval.

Note also that diffuse auroras are classified only when bright external sources (e.g., Moon or twilight) are absent, so the selected diffuse events are naturally free from such contamination and the red/blue ratio remains unaffected. However, this selection implies that the sample includes a mixture of diffuse auroral subtypes rather than exclusively pulsating auroras, so the

https://doi.org/10.5194/egusphere-2026-385
Preprint. Discussion started: 29 January 2026
© Author(s) 2026. CC BY 4.0 License.

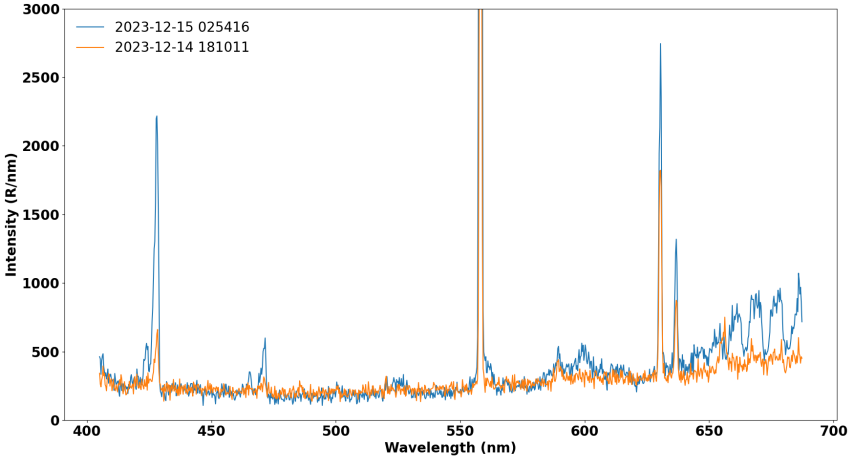

Figure 3. Two example ASIS spectra from the same night, showing a pre-midnight (softer in orange) and post-midnight (harder in blue) precipitation event.

inferred mean energies should be interpreted as effective averages over this mixed population. In addition, the 30 s integration time of the spectrograph averages over on–off pulsation cycles, which further reduces the apparent amplitude of the high-energy phases. Both effects probably lead to an underestimate of the true characteristic energy of the pulsating components, while preserving the statistical variability.

3 Results

3.1 Statistical Distribution of Median Energy with MLT

Figure 5 summarizes the statistical evolution of the median of the mean-energy as a function of magnetic local time (MLT). The lower panel shows the normalized distribution of median electron energy, binned in 300 eV intervals from 0.3 to 7.5 keV, while the upper panel displays the corresponding median energy and its variability, estimated using the median absolute deviation (MAD). The color scale in the heatmap represents the relative occurrence frequency of each energy bin within a given MLT hour. The use of the MAD instead of the standard deviation reflects the strongly non-Gaussian and asymmetric distribution of the inferred mean electron energies across the ensemble of spectra, resulting from the mixture of different diffuse auroral regimes (e.g. diffuse, pulsating, or patchy). The MAD thus provides a more robust measure of dispersion and limits the influence of occasional high-energy events.

Between 18 MLT and midnight, the emission is dominated by sub-3 keV electrons, with a strong occurrence peak near 2–2.5 keV. After midnight, the median energy progressively increases, with occurrence between 3 and 5 keV, peaking between 6 and 8 MLT. This trend indicates a systematic hardening of the electron population toward the dawn sector, consistent with

https://doi.org/10.5194/egusphere-2026-385
Preprint. Discussion started: 29 January 2026
© Author(s) 2026. CC BY 4.0 License.

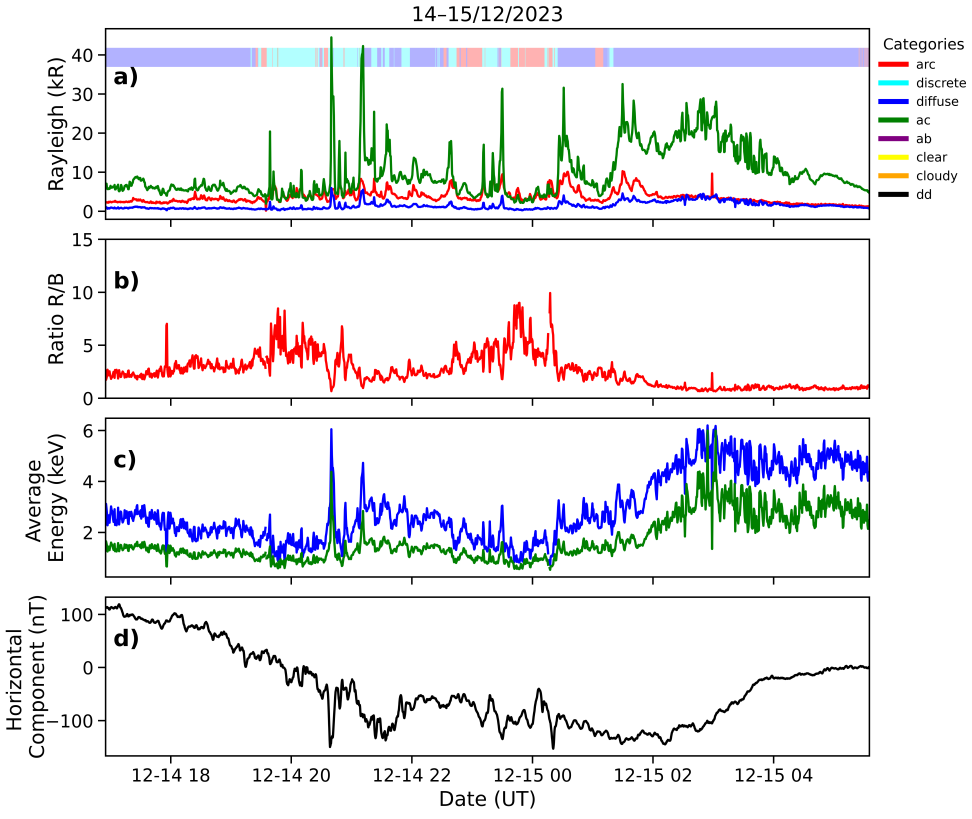

Figure 4. Results from ASIS for 14–15 December 2023. Panel a): green (557.7 nm), red-doublet (630/636 nm), and blue (427.8 nm) intensities, together with the AI-based morphology classification from Nanjo et al. (2022); Panel b): ratio between the 630 nm line emission and the 427.8 nm. Panel c): average energy using the look-up table from Adachi et al. (2017) in blue, and from Barthelemy et al. (2025) in green. Panel d): magnetic disturbance horizontal component from Tromsø magnetic observatory.

more efficient acceleration as the local time advances. The width of the distribution, represented by the MAD, remains fairly consistent throughout the night, indicating that the overall variability in precipitation energy does not change substantially with MLT. However, a slight enhancement in dispersion is visible near 5-6 MLT, possibly reflecting a more heterogeneous mix of auroral forms between patchy and non-patchy auroras (Ito et al., 2024).

3.2 Bayesian Assessment of the Energy Hardening

To quantitatively assess whether the observed increase in median energy represents a statistically significant trend, we applied a Bayesian piecewise linear regression model:

https://doi.org/10.5194/egusphere-2026-385
Preprint. Discussion started: 29 January 2026
© Author(s) 2026. CC BY 4.0 License.

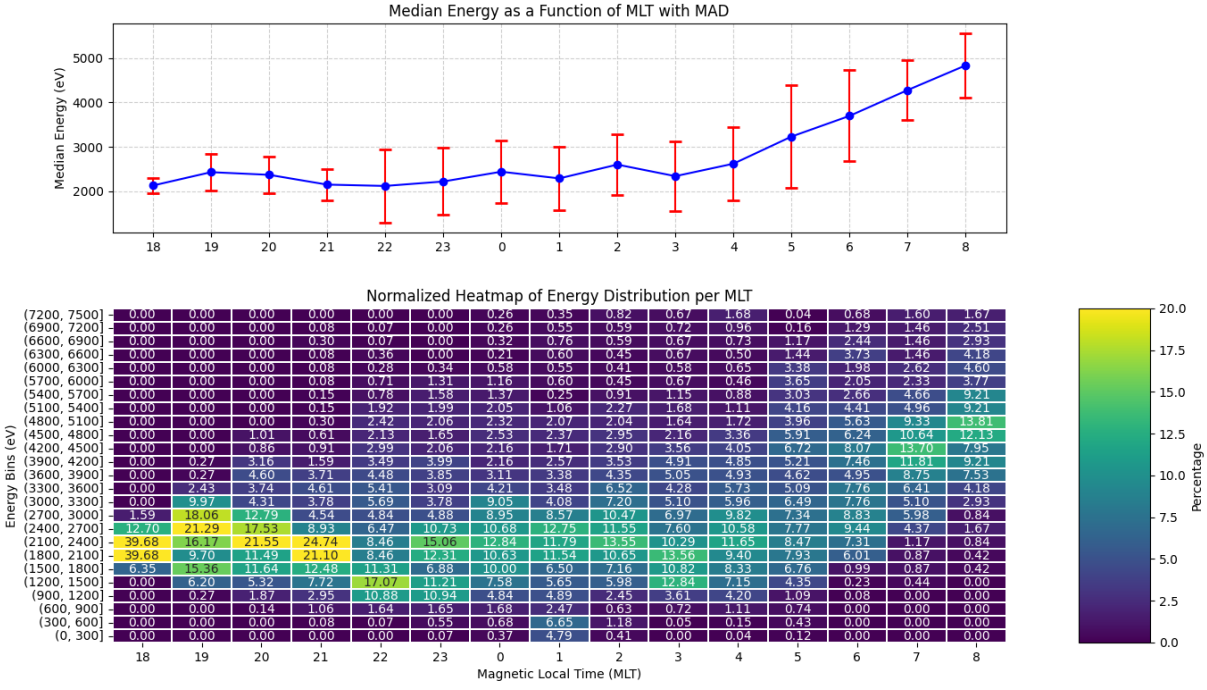

Figure 5. Top: median of the mean energy versus MLT with robust dispersion (MAD-based). Bottom: normalized energy–MLT heat map showing the progressive post-midnight hardening.

$$E_{\text{median}} = \beta_0 + \beta_1 \cdot \text{MLT} + \beta_2 \cdot (\text{MLT} - \text{breakpoint})_+ \tag{2}$$

The Bayesian framework was chosen because it allows for a probabilistic characterization of trends without relying on Gaussian assumptions or symmetric error distributions. Unlike classical regressions that return a single best-fit slope, the Bayesian approach provides a full posterior distribution for each parameter, quantifying the confidence that the observed energy increase is genuine or not. The goal is therefore to estimate the posterior distribution of the regression coefficients $\boldsymbol{\beta} = (\beta_0, \beta_1, \beta_2)$ and the dispersion term (σ_y), according to Bayes' theorem:

$$p(\boldsymbol{\beta}, \sigma_y \mid \text{data}) \propto p(\text{data} \mid \boldsymbol{\beta}, \sigma_y) p(\boldsymbol{\beta}, \sigma_y) \tag{3}$$

Here, the likelihood

$$p(\text{data} \mid \boldsymbol{\beta}, \sigma_y)$$

https://doi.org/10.5194/egusphere-2026-385
Preprint. Discussion started: 29 January 2026
© Author(s) 2026. CC BY 4.0 License.

expresses the probability of observing the data given a particular set of parameters, including the σ_y^2 term representing the observational scatter around the median. The energy distributions are markedly non-Gaussian, since we are mixing different auroral events, its value was not estimated as a standard deviation. Instead, a robust scale estimator was used, defined as 1.4826 MAD, which corresponds to the Gaussian-equivalent standard deviation. The prior term

$$p(\boldsymbol{\beta}, \sigma_y)$$

encodes weak prior knowledge about the parameters, serving mainly to regularize the inference and constrain the model to physically reasonable ranges, according to Figure 5. In this study, we used broad normal priors centered on plausible physical values

$$\beta_0 \sim \mathcal{N}(2000, 1000^2)$$

and

$$\beta_1, \beta_2 \sim \mathcal{N}(0, 500^2)$$

which allows the data to dominate the posterior.

Posterior estimation was performed using the No-U-Turn Sampler (NUTS), a gradient-based Markov Chain Monte Carlo (MCMC) algorithm implemented in PyMC. Each iteration proposes new values of the parameters conditional on the data: candidate sets that better reproduce the observed median energies under the normal likelihood are assigned a higher posterior probability. After 8000 iterations, the Markov chain converges toward the stationary posterior distribution, where the frequency of sampled parameter values reflects their relative plausibility.

Figure 6 illustrates the Bayesian analysis of the median electron energy as a function of magnetic local time (MLT). The left panel shows the observed median energies (black points, with robust dispersion σ = 1.4826 × MAD as vertical bars) and the posterior median energy trend (blue line), together with its 95% credible interval (blue shading). The right panel displays the posterior distribution of the slope β_2, which quantifies the change in the energy–MLT slope after the 4 MLT break point.

The inferred posterior median slope increment is β_2 = 455 $\pm$ 246 eV per MLT, with a 95% highest-density interval (HDI) spanning from –14 to 944 eV per MLT. The posterior probability of a positive slope, P(β_2 >0) = 0.97 indicates that an increase in the median energy after midnight is strongly supported, although the 95% HDI marginally includes zero. This indicates a strong likelihood that the median electron energy increases systematically after midnight. Indeed, this analysis therefore supports the interpretation that the dawnside hardening of the electron precipitation is not an artifact of statistical dispersion, but a genuine physical feature of the nightside-to-dawn transition. Quantitatively, the inferred trend corresponds to an approximate doubling of the median energy between midnight ($\approx$ 2.5 keV) and 8 MLT ($\approx$ 5 keV).

3.3 Discussion of variability

The apparent spread in the inferred energies must be interpreted in view of the observational limitations discussed in Section 2.2. Spatial and temporal averaging caused by the small field of view and the 30 s exposure time smooths the mean energy

https://doi.org/10.5194/egusphere-2026-385
Preprint. Discussion started: 29 January 2026
© Author(s) 2026. CC BY 4.0 License.

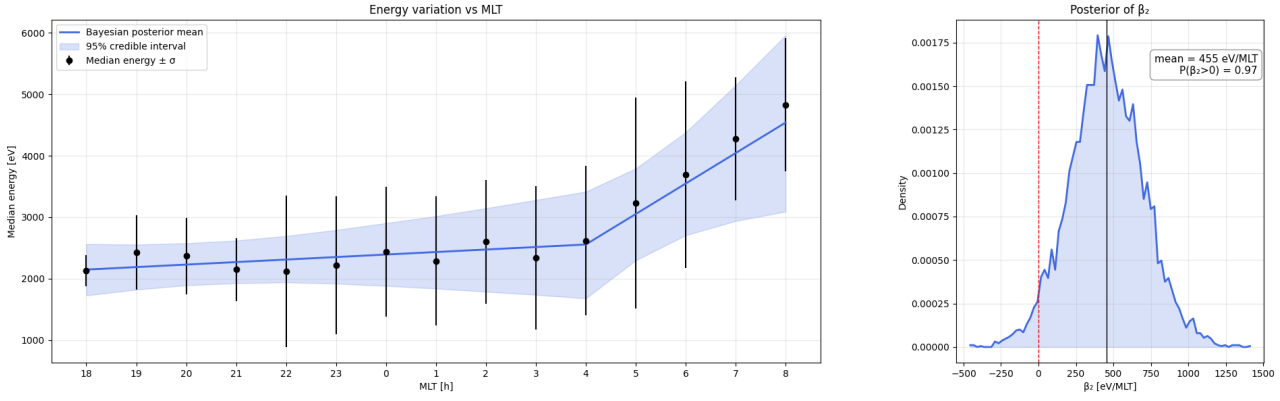

Figure 6. Bayesian regression of the MLT-dependent energy trend. Left: posterior median and 95% credible interval. Right: posterior distribution of the post-midnight slope parameter β_2

and mixes different diffuse auroral morphologies. This leads to a broader energy distribution and a lower median compared to purely pulsating events. The large median absolute deviations (MADs) found across all MLT sectors therefore likely reflect genuine variability in diffuse precipitation rather than measurement noise, justifying the use of robust statistics.

It is important to once again emphasize that the inferred electron energies presented in this study, based on line intensity ratios, are only approximations. Our analysis is therefore best interpreted in a statistical context, that captures general trends in the hardness of electron precipitation: the observed increase in mean energy near 03–04 MLT is robust across the large dataset, but the absolute energy values should be regarded with caution. Future works should incorporate full-spectrum modeling and altitude-dependent radiative transfer that could provide more precise estimates of characteristic mean energy and energy flux as performed by Barthelemy et al. (2025).

4 Dependence on the AE index

The Auroral Electrojet (AE) index is a standard geomagnetic indicator of substorm activity in the auroral zone (Akasofu, 1964; Davis and Sugiura, 1966). While AE is a global rather than local index, it remains a widely used proxy for magnetospheric activity in statistical analyses. In this study, AE values were obtained from the World Data Center for Geomagnetism, Kyoto (https://wdc.kugi.kyoto-u.ac.jp), with a time resolution of 1 minute. For each 30 s spectrograph measurement, the corresponding AE value was obtained using a nearest-neighbor approach, taking advantage of the smooth temporal variability of the 1-minute AE index, which has an autocorelation time of 285 minutes (Maggiolo et al., 2017). Meredith et al. (2020) showed that the magnetic amplitude of whistler-mode chorus increases markedly with AE, providing a direct link between geomagnetic activity and the efficiency of wave-driven electron scattering. Since chorus occurrence is naturally enhanced on the postmidnight–dawn side, AE-dependent changes in wave power are expected to modulate the hardness of precipitating electrons in this MLT sector. The AE index (1-minute cadence) was used to categorize geomagnetic activity into three bins: a “quiet” state for

https://doi.org/10.5194/egusphere-2026-385
Preprint. Discussion started: 29 January 2026
© Author(s) 2026. CC BY 4.0 License.

AE < 100 nT, an "intermediate" or weakly disturbed state for 100–300 nT, and an "active" regime for AE > 300 nT, following the approach of Meredith et al. (2020).

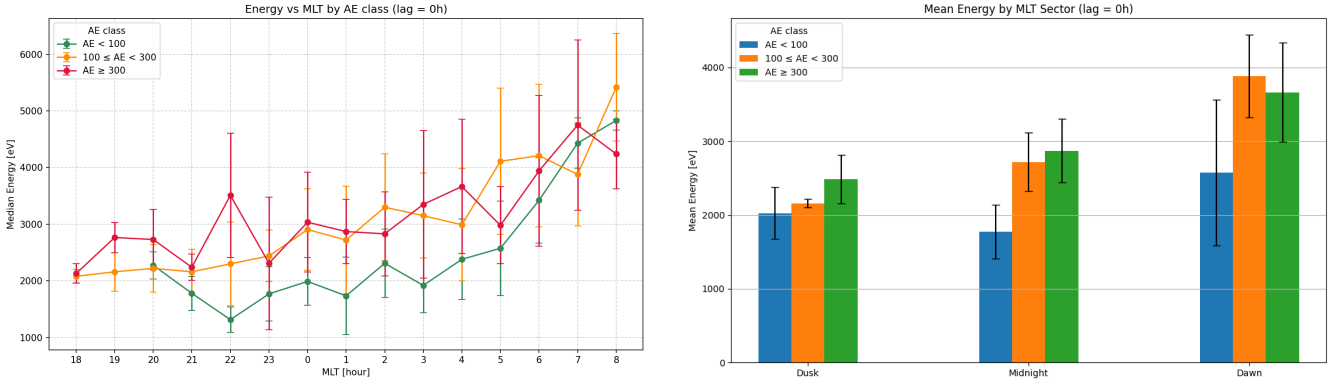

(a) Median of the mean energy versus MLT for three AE activity levels

(b) Sector-averaged median energy (dusk, midnight, dawn) for each AE class

Figure 7. MLT dependence of diffuse-aurora precipitation energy under three geomagnetic activity levels. Panel (a) shows hourly median energies; panel (b) shows the sector-averaged median energies.

4.1 Instantaneous AE (lag = 0 h)

Figure 7a shows the median of the mean energy as a function of MLT for the three AE classes without temporal lag, with 8167, 8177, and 4613 spectra for $\mathrm{AE} < 100$ nT, $100 \leq \mathrm{AE} < 300$ nT, and $\mathrm{AE} \geq 300$ nT, respectively.

For AE < 100 nT, the increase in the median toward the dawn sector is the clearest and most consistent. The Bayesian analysis yields a posterior probability $P(\beta_2 > 0) = 0.996$ (Table 1), indicating a robust post-midnight hardening. Under such quiet conditions, the events classified as "diffuse" (AI probability > 75%) are statistically the most representative of wave-driven precipitation, in particular chorus-related diffuse and pulsating aurora. With minimal contamination from injections or dynamic discrete structures, the underlying MLT-dependent hardening remains well defined.

For $100 \leq$ AE < 300 nT, the trend remains visible but is noticeably less pronounced. In this intermediate regime, the diffuse aurora class begins to include a broader mixture of precipitation types, including weakly structured diffuse patches and soft electron precipitation associated with mild injections near midnight. This broader range of auroral forms is associated with larger variability in the inferred energies, which reduces the clarity of the MLT dependence.

For $\mathrm{AE} \geq 300$ nT, the relation becomes more scattered. Stronger geomagnetic activity introduces frequent particle injections, bright discrete arcs, and post-substorm structures, some of which can enter the diffuse category even with an AI probability threshold of 75%. The resulting sample is therefore more heterogeneous, and the MLT-dependent hardening becomes more difficult to isolate, which is confirmed by the P(β_2) of 0.78.

https://doi.org/10.5194/egusphere-2026-385
Preprint. Discussion started: 29 January 2026
© Author(s) 2026. CC BY 4.0 License.

To further reduce the noise introduced by hour-by-hour variability, the observations were also grouped into three broad MLT sectors: dusk ($18 \leq$ MLT < 22), midnight ($22 \leq$ MLT < 3), and dawn ($3 \leq$ MLT ≤ 8). The corresponding sector-averaged median energies for each AE class are presented in Fig. 7b. This sector-based view confirms that, for all AE classes, the highest median of the mean energies are consistently observed in the dawn sector, reflecting a persistent MLT-dependent hardening.

Table 1. Bayesian inference of the post-midnight energy increase (slope parameter β_2) for the three AE activity classes, using the median energy per MLT bin. The uncertainties correspond to the standard deviation of the posterior samples, and the last column reports the 95% highest-density interval (HDI).

AE class	$P(\beta_2 > 0)$	β_2 [eV/MLT]	95% HDI [eV/MLT]
AE $<$ 100 nT	0.996	581.5 ± 229.4	[142, 1033]
$100 \leq$ AE $<$ 300 nT	0.814	302.1 ± 338.6	$[-376, 940]$
AE $\geq$ 300 nT	0.780	250.8 ± 320.5	$[-375, 864]$

4.2 Magnetospheric memory: AE with temporal lags

Diffuse auroral precipitation does not respond instantaneously to variations in geomagnetic activity. We also examined the AE index at different temporal lags relative to each spectrograph measurement. As discussed by Hosokawa and Ogawa (2015), particle scattering and wave–particle interactions are influenced not only by the instantaneous state of the magnetosphere but also by the prior accumulation of energy and tail stretching during preceding hours. In particular, substorm-related enhancements of AE reflect the growth and release of magnetic energy in the magnetotail, which can modulate the flux and energy of precipitating electrons long after the peak of the electrojet activity. Evaluating AE at lags from 0 h to 24 h therefore allows us to assess whether the observed MLT-dependent hardening of the median electron energy is primarily controlled by the immediate auroral electrojet activity or by the cumulative magnetospheric conditions leading up to it.

When using a 2-h lag, the number of events classified as quiet (AE $<$ 100 nT) drops from 8167 to 2589. This indicates that, although many spectra are recorded at times when AE(t) is below 100 nT, a substantial fraction of them are preceded within the last two hours by intervals of enhanced activity (AE $\geq$ 100 nT). As a consequence, the Bayesian posterior probability for a positive slope in the AE $<$ 100 nT class decreases from 0.996 (lag = 0 h) to about 0.75. At the same time, the class $100 \leq$ AE $<$ 300 nT exhibits a strengthened slope with $P(\beta_2 > 0) \approx 0.98$. This does not contradict the original trend; instead, it shows that many intervals with low AE(t) do not correspond to genuinely quiet conditions but to a magnetosphere still recovering from earlier activity.

For a 24-h lag, nearly all events fall into the AE ≥ 300 nT class, confirming that diffuse and pulsating auroras predominantly occur when the magnetosphere has been moderately or strongly preconditioned. The situation is then similar to that shown in Fig 6. The magnetosphere is then rarely in a truly undisturbed state over multi-hour timescales, and the precipitation at a given time often reflects the memory of recent injections and chorus enhancement rather than the instantaneous AE only. Intervals

https://doi.org/10.5194/egusphere-2026-385
Preprint. Discussion started: 29 January 2026
© Author(s) 2026. CC BY 4.0 License.

that remain in the AE < 100 nT class even with a 2-h memory therefore correspond to genuinely quiet, weakly preconditioned conditions, and do not show a particular positive energy–MLT trend.

5 Discussion

This study provides a statistical characterization of the evolution of the characteristic electron precipitation energy as a function of magnetic local time (MLT) for diffuse auroras, including pulsating auroras as a major subcategory. Using two winter seasons of ground-based spectroscopic observations with the ASIS instrument, we confirm a systematic hardening of the precipitating electron population after midnight. The two-wavelength method reveals an increase of the median characteristic energy from approximately 2–2.5 keV near midnight to values approaching 5 keV toward the dawn sector. By combining this MLT analysis with a Bayesian statistical framework, we show that this trend is robust when evaluated on the median energy while accounting for the non-Gaussian dispersion of the energy distributions. Within this framework, the onset of precipitation hardening is most consistently observed near 04 MLT. This behavior is observed both in the analysis of the full dataset and in analyses conditioned on geomagnetic activity, and is therefore unlikely to result solely from sampling effects. In addition, the dependence on geomagnetic activity indicates that the hardening persists under quiet conditions but becomes more structured when geomagnetic activity is considered using time-lagged AE indices, highlighting the role of magnetospheric preconditioning.

The post-midnight hardening of electron precipitation identified in this study is broadly consistent with earlier observational results based on optical imaging, radar measurements, and satellite observations. Several previous studies have reported a dawnward evolution toward harder precipitation, often inferred from changes in emission altitude or occurrence statistics. Using incoherent-scatter radar observations, Hosokawa and Ogawa (2015) reported a systematic decrease in the peak emission altitude of pulsating auroras after magnetic midnight, indicative of progressively harder electron precipitation in the post-midnight sector. Statistical studies based on all-sky imager observations by Partamies et al. (2017) similarly showed that pulsating auroras predominantly occur between approximately 02 and 06 MLT, consistent with enhanced energetic precipitation in the morning sector. More quantitative indications of a transition were reported by Kawamura et al. (2020) and Nanjo et al. (2021), who showed that the hardest precipitation or lowest emission altitudes tend to occur after approximately 03–04 MLT. These results are consistent with the post-midnight hardening identified in the present study.

Several mechanisms have been proposed to explain this post-midnight hardening of electron precipitation. A widely discussed framework is provided by the kinetic modeling study of Miyoshi et al. (2015), who showed that lower-band chorus waves can preferentially scatter higher-energy electrons into the atmospheric loss cone. Although chorus waves are generated near the magnetic equator, their propagation to higher magnetic latitudes along magnetic field lines modifies the resonance conditions by reducing the local electron cyclotron frequency and altering the parallel wave number. These effects shift the cyclotron resonance toward higher-energy electrons, resulting in harder precipitation. Recent observational work by Ito et al. (2024) supports this interpretation by demonstrating that chorus waves observed in the dawn sector tend to occur in regions with lower local electron cyclotron frequencies and exhibit larger $k_{\|}$ values than those observed closer to midnight. These wave properties naturally favor resonance with higher-energy electrons, providing a plausible explanation for the observed increase

https://doi.org/10.5194/egusphere-2026-385
Preprint. Discussion started: 29 January 2026
© Author(s) 2026. CC BY 4.0 License.

in characteristic precipitation energy toward dawn. The consistency between the onset MLT identified in this study and the MLT dependence of chorus wave properties reported by Ito et al. (2024) suggests that changes in wave–particle interaction conditions play a central role in shaping the observed energy evolution.

6 Conclusion

Using two winter seasons of high-cadence ground-based spectroscopic observations, this study provides a robust statistical characterization of the magnetic local time dependence of diffuse auroral electron precipitation energy. The results confirm a systematic post-midnight hardening of the precipitating electron population, with characteristic energies increasing toward the dawn sector. The onset of this hardening is identified near 04 MLT and persists across geomagnetic activity levels, indicating that it represents a genuine physical feature of diffuse auroral precipitation rather than an artifact of sampling or analysis.

Although several observational limitations tend to bias the retrieved energies toward lower values, the observed trends remain consistent and statistically significant. These results complement previous optical, radar, and satellite studies and provide new quantitative constraints on the timing and magnitude of electron precipitation hardening. Overall, the ASIS observations highlight the potential of ground-based auroral spectroscopy to investigate long-term statistical properties of wave-driven precipitation processes in the nightside magnetosphere.

Data availability. All-sky color camera images are available at http://darndeb08.cei.uec.ac.jp/~nanjo/public/skibotn_imgs/. The inferred mean electron energies derived from the ASIS spectra for all diffuse auroral events analyzed in this study are publicly available at https://asis.aeronomie.be/papers

Author contributions. G.C. and K.H. conceived the study. G.C. developed the data-analysis code and led the manuscript writing. G.C., H.L., and M.B. performed the calibration of the ASIS data. S.N. provided the AI-based auroral classification. M.G.J. provided the magnetometer data and contributed to its interpretation. R.M. and G.C. analyzed the dependence on the AE index. All authors contributed to the scientific discussion and interpretation of the results and reviewed the manuscript.

Competing interests. At least one of the (co-)authors is a member of the editorial board of Annales Geophysicae.

Acknowledgements. GC is funded by the Solar-Terrestrial Center of Excellence (STCE). SN was supported by the Japan Society for the Promotion of Science (JSPS) Overseas Research Fellowships. KH is supported by the Japan Society for the Promotion of Science (JSPS) Kakenhi 22H00173. KH was supported by the STCE Visitors Program, which funded a research visit in March 2025. The authors disclose

https://doi.org/10.5194/egusphere-2026-385
Preprint. Discussion started: 29 January 2026
© Author(s) 2026. CC BY 4.0 License.

that generative AI was used for language editing and formatting assistance, and to develop the data-analysis code; all scientific content, analyses, and conclusions were produced and verified by the authors.

https://doi.org/10.5194/egusphere-2026-385
Preprint. Discussion started: 29 January 2026
© Author(s) 2026. CC BY 4.0 License.

References

Adachi, K., Nozawa, S., Ogawa, Y., Brekke, A., Hall, C., and Fujii, R.: Evaluation of a method to derive ionospheric conductivities using two auroral emissions (428 and 630 nm) measured with a photometer at Tromsø (69.6°N), Earth, Planets and Space, 69, 90, https://doi.org/10.1186/s40623-017-0677-4, 2017.

Akasofu, S.-I.: The development of the auroral substorm, Planetary and Space Science, 12, 273–282, https://doi.org/10.1016/0032-0633(64)90151-5, 1964.

Barthelemy, M., Robert, E., and Lamy, H.: Synthetic spectra of the aurora: N2, N2+, N, N+, O2+ and O emissions, J. Space Weather Space Clim., 15, 19, https://doi.org/10.1051/swsc/2025013, 2025.

Davis, T. N. and Sugiura, M.: Auroral electrojet activity index AE and its universal time variations, Journal of Geophysical Research, 71, 785–801, https://doi.org/10.1029/JZ071i003p00785, 1966.

Donovan, E., Mende, S., Jackel, B., Frey, H., Syrjäsuo, M., Voronkov, I., Trondsen, T., Peticolas, L., Angelopoulos, V., Harris, S., Greffen, M., and Connors, M.: The THEMIS all-sky imaging array—system design and initial results from the prototype imager, Journal of Atmospheric and Solar-Terrestrial Physics, 68, 1472–1487, https://doi.org/https://doi.org/10.1016/j.jastp.2005.03.027, passive Optics Aeronomy, 2006.

Fukizawa, M., Sakanoi, T., Miyoshi, Y., Kazama, Y., Katoh, Y., Kasahara, Y., Matsuda, S., Matsuoka, A., Kurita, S., Shoji, M., Teramoto, M., Imajo, S., Sinohara, I., Wang, S.-Y., Tam, S. W.-Y., Chang, T.-F., Wang, B.-J., and Jun, C.-W.: Pitch-Angle Scattering of Inner Magnetospheric Electrons Caused by ECH Waves Obtained With the Arase Satellite, Geophysical Research Letters, 47, e2020GL089 926, https://doi.org/https://doi.org/10.1029/2020GL089926, e2020GL089926 2020GL089926, 2020.

Grono, E. and Donovan, E.: Differentiating diffuse auroras based on phenomenology, Annales Geophysicae, 36, 891–898, https://doi.org/10.5194/angeo-36-891-2018, 2018.

Hosokawa, K. and Ogawa, Y.: Ionospheric variation during pulsating aurora, Journal of Geophysical Research (Space Physics), 120, 5943–5957, https://doi.org/10.1002/2015JA021401, 2015.

Hosokawa, K., Miyoshi, Y., Ozaki, M., Oyama, S.-I., Ogawa, Y., Kurita, S., Kasahara, Y., Kasaba, Y., Yagitani, S., Matsuda, S., Tsuchiya, F., Kumamoto, A., Kataoka, R., Shiokawa, K., Raita, T., Turunen, E., Takashima, T., Shinohara, I., and Fujii, R.: Multiple time-scale beats in aurora: precise orchestration via magnetospheric chorus waves, Scientific Reports, 10, 3380, https://doi.org/10.1038/s41598-020-59642-8, 2020.

Hosokawa, K., Oyama, S.-I., Ogawa, Y., Miyoshi, Y., Kurita, S., Teramoto, M., Nozawa, S., Kawabata, T., Kawamura, Y., Tanaka, Y.-M., Miyaoka, H., Kataoka, R., Shiokawa, K., Brändström, U., Turunen, E., Raita, T., Johnsen, M. G., Hall, C., Hampton, D., Ebihara, Y., Kasahara, Y., Matsuda, S., Shinohara, I., and Fujii, R.: A Ground-Based Instrument Suite for Integrated High-Time Resolution Measurements of Pulsating Aurora With Arase, Journal of Geophysical Research: Space Physics, 128, e2023JA031 527, https://doi.org/https://doi.org/10.1029/2023JA031527, e2023JA031527 2023JA031527, 2023.

Ito, Y., Hosokawa, K., Ogawa, Y., Miyoshi, Y., Tsuchiya, F., Fukizawa, M., Kasaba, Y., Kazama, Y., Oyama, S., Murase, K., Nakamura, S., Kasahara, Y., Matsuda, S., Kasahara, S., Hori, T., Yokota, S., Keika, K., Matsuoka, A., Teramoto, M., and Shinohara, I.: On the Factors Controlling the Relationship Between Type of Pulsating Aurora and Energy of Pulsating Auroral Electrons: Simultaneous Observations by Arase Satellite, Ground-Based All-Sky Imagers and EISCAT Radar, Journal of Geophysical Research: Space Physics, 129, e2024JA032 617, https://doi.org/https://doi.org/10.1029/2024JA032617, e2024JA032617 2024JA032617, 2024.

https://doi.org/10.5194/egusphere-2026-385
Preprint. Discussion started: 29 January 2026
© Author(s) 2026. CC BY 4.0 License.

Kasahara, S., Yokota, S., Mitani, T., Asamura, K., Hirahara, M., Miyoshi, Y., Kazama, Y., Tsuchiya, F., Matsuda, S., Kasaba, Y., Saito, Y., Takashima, T., and Fujimoto, M.: Pulsating aurora from electron scattering by chorus waves, Nature, 554, 337–340, https://doi.org/10.1038/nature25505, 2018.

Kawamura, S., Nishiyama, T., Kataoka, R., Ogawa, Y., Sato, Y., Tsuda, T., Kurita, S., and Saito, Y.: Energy characteristics of pulsating auroras derived from all-sky camera observations, Earth, Planets and Space, 72, 168, https://doi.org/10.1186/s40623-020-01229-8, 2020.

Maggiolo, R., Hamrin, M., De Keyser, J., Pitkänen, T., Cessateur, G., Gunell, H., and Maes, L.: The Delayed Time Response of Geomagnetic Activity to the Solar Wind, Journal of Geophysical Research: Space Physics, 122, 11,109–11,127, https://doi.org/https://doi.org/10.1002/2016JA023793, 2017.

Meredith, N. P., Horne, R. B., Bortnik, J., Li, W., Shen, X., Vellante, M., Piersanti, M., Magnes, W., Nakamura, R., and Santolík, O.: Global Model of Whistler Mode Chorus in the Near-Equatorial Region: Dependence on Geomagnetic Activity, Geophysical Research Letters, 47, e2020GL087 311, https://doi.org/10.1029/2020GL087311, 2020.

Miyoshi, Y., Saito, S., Seki, K., Nishiyama, T., Kataoka, R., Asamura, K., Katoh, Y., Ebihara, Y., Sakanoi, T., Hirahara, M., Oyama, S., Kurita, S., and Santolik, O.: Relation between fine structure of energy spectra for pulsating aurora electrons and frequency spectra of whistler mode chorus waves, Journal of Geophysical Research: Space Physics, 120, 7728–7736, https://doi.org/https://doi.org/10.1002/2015JA021562, 2015.

Nanjo, S., Hozumi, Y., Hosokawa, K., Kataoka, R., Miyoshi, Y., Oyama, S.-i., Ozaki, M., Shiokawa, K., and Kurita, S.: Periodicities and Colors of Pulsating Auroras: DSLR Camera Observations From the International Space Station, Journal of Geophysical Research: Space Physics, 126, e2021JA029 564, https://doi.org/https://doi.org/10.1029/2021JA029564, e2021JA029564 2021JA029564, 2021.

Nanjo, S., Kataoka, R., Nishiyama, T., Yoneda, M., and Miyaoka, H.: Automatic classification of auroral morphology from all-sky images by using a convolutional neural network, Scientific Reports, 12, 7883, https://doi.org/10.1038/s41598-022-11686-8, 2022.

Nanjo, S., Ebukuro, S., Nakamura, S., Miyoshi, Y., Kurita, S., Oyama, S.-I., Ogawa, Y., Keika, K., Kasahara, Y., Kasahara, S., Matsuoka, A., Hori, T., Yokota, S., Matsuda, S., Shinohara, I., Wang, S.-Y., Kazama, Y., Jun, C.-W., Kitahara, M., and Hosokawa, K.: An Implication of Detecting the Internal Modulation in a Pulsating Aurora: A Conjugate Observation by the Arase Satellite and All-Sky Imagers, Journal of Geophysical Research: Space Physics, 128, e2023JA031 499, https://doi.org/https://doi.org/10.1029/2023JA031499, e2023JA031499 2023JA031499, 2023.

Newell, P. T., Sotirelis, T., and Wing, S.: Diffuse, monoenergetic, and broadband aurora: The global precipitation budget, Journal of Geophysical Research: Space Physics, 114, https://doi.org/https://doi.org/10.1029/2009JA014326, 2009.

Nishimura, Y., Bortnik, J., Li, W., Thorne, R. M., Lyons, L. R., Angelopoulos, V., Mende, S. B., Bonnell, J. W., Contel, O. L., Cully, C., Ergun, R., and Auster, U.: Identifying the Driver of Pulsating Aurora, Science, 330, 81–84, https://doi.org/10.1126/science.1193186, 2010a.

Nishimura, Y., Lyons, L. R., Angelopoulos, V., and Donovan, E. F.: Substorm triggering by new plasma intrusion: THEMIS all-sky imager observations, Journal of Geophysical Research: Space Physics, 115, A07 222, https://doi.org/10.1029/2009JA015166, 2010b.

Nishimura, Y., Lessard, M. R., Katoh, Y., Miyoshi, Y., Grono, E., Partamies, N., Sivadas, N., Hosokawa, K., Fukizawa, M., Samara, M., Michell, R. G., Kataoka, R., Sakanoi, T., Whiter, D. K., Oyama, S.-i., Ogawa, Y., and Kurita, S.: Diffuse and Pulsating Aurora, Space Science Reviews, 216, 4, https://doi.org/10.1007/s11214-019-0629-3, 2020.

Nozawa, S., Kawabata, T., Hosokawa, K., Ogawa, Y., Tsuda, T., Mizuno, A., Fujii, R., and Hall, C.: A new five-wavelength photometer operated in Tromsø (69.6°N, 19.2°E), Earth, Planets and Space, 70, 193, https://doi.org/10.1186/s40623-018-0962-x, 2018.

https://doi.org/10.5194/egusphere-2026-385
Preprint. Discussion started: 29 January 2026
© Author(s) 2026. CC BY 4.0 License.

Ozaki, M., Yagitani, S., Ishizaka, K., Shiokawa, K., Miyoshi, Y., Kadokura, A., Yamagishi, H., Kataoka, R., Ieda, A., Ebihara, Y., Sato, N., and Nagano, I.: Observed correlation between pulsating aurora and chorus waves at Syowa Station in Antarctica: A case study, Journal of Geophysical Research: Space Physics, 117, https://doi.org/https://doi.org/10.1029/2011JA017478, 2012.

Ozaki, M., Miyoshi, Y., Shiokawa, K., Hosokawa, K., Oyama, S.-i., Kataoka, R., Ebihara, Y., Ogawa, Y., Kasahara, Y., Yagitani, S., Kasaba, Y., Kumamoto, A., Tsuchiya, F., Matsuda, S., Katoh, Y., Hikishima, M., Kurita, S., Otsuka, Y., Moore, R. C., Tanaka, Y., Nosé, M., Nagatsuma, T., Nishitani, N., Kadokura, A., Connors, M., Inoue, T., Matsuoka, A., and Shinohara, I.: Visualization of rapid electron precipitation via chorus element wave–particle interactions, Nature Communications, 10, 257, https://doi.org/10.1038/s41467-018-07996-z, 2019.

Partamies, N., Weygand, J. M., Whiter, D. K., Syrjäsuo, M., Donovan, E., and Nishimura, Y.: Occurrence and average behavior of pulsating aurora, Journal of Geophysical Research: Space Physics, 122, 5606–5618, https://doi.org/10.1002/2016JA023513, 2017.

Royrvik, O. and Davis, T. N.: Pulsating aurora: Local and global morphology, Journal of Geophysical Research (1896-1977), 82, 4720–4740, https://doi.org/https://doi.org/10.1029/JA082i029p04720, 1977.

Solomon, S. C.: Global modeling of thermospheric airglow in the far ultraviolet, Journal of Geophysical Research: Space Physics, 122, 7834–7848, https://doi.org/https://doi.org/10.1002/2017JA024314, 2017.

Tsuruda, K., Machida, S., Oguti, T., Kokubun, S., Hayashi, K., Kitamura, T., Saka, O., and Watanabe, T.: Correlations between the very low frequency chorus and pulsating aurora observed by low-light-level television at, Canadian Journal of Physics, 59, 1042–1048, https://doi.org/10.1139/p81-137, 1981.

Yamamoto, T.: On the temporal fluctuations of pulsating auroral luminosity, Journal of Geophysical Research: Space Physics, 93, 897–911, https://doi.org/https://doi.org/10.1029/JA093iA02p00897, 1988.